Article

Hybrid Polymer–Inorganic Coatings Enriched with Carbon Nanotubes on Ti-6Al-4V Alloy for Biomedical Applications

Dominika Träger, Dagmara Słota *, Karina Niziołek, Wioletta Florkiewicz and Agnieszka Sobczak-Kupiec

Department of Materials Engineering, Faculty of Materials Engineering and Physics, Cracow University of Technology, 37 Jana Pawła II Av., 31-864 Krakow, Poland; dominika.trager@student.pk.edu.pl (D.T.); karina.niziolek@doktorant.pk.edu.pl (K.N.); agnieszka.sobczak-kupiec@pk.edu.pl (A.S.-K.)
* Correspondence: dagmara.slota@doktorant.pk.edu.pl

Abstract: Bone tissue degeneration, caused by disease as well as trauma, is a problem affecting many social groups in the 21st century. It involves pain and reduced patient comfort. Developments in materials engineering allow for the design of novel, innovative materials that can be used in therapies to promote bone regeneration. This work presents the preparation of a ceramic–polymer coating modified with carbon nanotubes on a titanium alloy for biomedical applications. The ceramic part is hydroxyapatite synthesized by the wet precipitation method using orthophosphate and calcium hydroxide. The polymer of choice was polyethylene glycol. A UV light synthesis method was successfully applied to obtain coatings characterized by continuity and full crosslinking. Extensive physicochemical analysis and incubation studies were carried out. Interactions between coatings and fluids mimicking artificial biological environments were analyzed for 9 days, i.e., in fluids such as SBF solution, artificial saliva, and distilled water. During the in vitro incubation, changes in pH values were measured by potentiometric tests, and ionic conductivity was measured by analyzing conductometry. After incubation, the surface morphology was studied by scanning electron microscopy (SEM) together with energy-dispersive (EDS) microanalysis, which made it possible to determine the presence of individual elements on the surface, as well as to observe the appearance of new apatite layers. Fourier-transform infrared (FT-IR) spectrometry was also performed before and at the end of the incubation period. On the basis of the presented studies, it was concluded that coatings that contain nanotubes are bioactive and do not negatively affect the properties of the coatings. Bioactivity was confirmed microscopically by observing new apatite layers after incubation in SBF, which were identified as phosphorus and calcium deposits. Degradation of the polymer phase was observed in the artificial saliva. These materials require further study, including safety analysis, but they demonstrate potential for further work.

Keywords: composites; coatings; polyethylene glycol; hydroxyapatite; carbon nanotubes

1. Introduction

The role of a supporting structure in the human body is played by bones, which are connective and supportive tissues. They consist of three types of cells: osteoblasts, osteoclasts, and osteocytes. In addition, they include collagen fibers and compounds of elements such as calcium, phosphorus, and magnesium. The cells that create bone are responsible for its remodeling, which is necessary to maintain its normal mechanical properties [1].

Unfortunately, bone tissue can be destroyed by injury or disease. Bone overload syndrome refers to bone tissue damage that occurs as a result of prolonged fatigue. It is characterized by the appearance of cracks or fractures, accompanied by pain. Stress fractures are associated with overtraining, so the groups most often affected are athletes [2].

In the aging population, more people are suffering due to osteoporosis. This disease causes a decrease in the strength of bone tissue, causing bone fragility. Lack of adequate

micronutrient supplementation, insufficient exercise, and advanced age increase the risk of this disease [3].

In order to accelerate bone regeneration and to fill defects caused by degradation, a frequently used material is hydroxyapatite (HA), with the chemical formula $Ca_{10}(PO_4)_6(OH)_2$. Thanks to its calcium and phosphorus content, HA is a highly biocompatible material and is biomimetic to the inorganic part of natural tissue [4]. Its advantages also include its bioactivity. Hydroxyapatite bonds well to bone tissue and promotes cell adhesion [5–7]. In addition, HA combines well with other biomaterials, forming a combination with high bioactive properties [8].

Polyethylene glycol (PEG) is a synthetic polymer belonging to the polyether group, formed by ethylene oxide polymerization [9]. It is biocompatible, non-toxic, non-immunogenic, and amphipathic, which makes it useful for biomaterials research and as a drug carrier [10]. Its long hydrophilic chain helps biodegrade the composite [11].

To improve the mechanical properties of a ceramic–polymer interface, the recommended additive is a titanium (90%) aluminum (6%) vanadium (4%) alloy (Ti-6Al-4V). It has excellent biocompatibility and corrosion resistance in physiological environments, as well as a low modulus of plasticity. Thanks to these properties, Ti-6Al-4V alloy is often used as a load-bearing implant following the reduction of shielding stress [12–16]. Therefore, it has found applications in orthopedic surgery [17,18]. Furthermore, titanium improves cell adhesion and supports cell proliferation [19,20]. This is a very important aspect in the creation of a material to promote bone tissue regeneration. Positive effects of combining Ti-6AL-4V with HA have also been reported [8].

An interesting material that blends very well with HA and synthetic or natural polymers are carbon nanotubes (CNTs) [21–23]. Made of graphene, the thinnest material in existence, they are classified into single-walled nanotubes (SWCNTs) and multi-walled nanotubes (MWCNTs), and they find applications in many scientific fields [24,25]. They are characterized by very good mechanical properties, such as high strength and flexibility [22,26]. The use of carbon nanotubes in tissue engineering is made possible by their biocompatibility and lack of toxicity in their interactions with cells [27,28]. When CNTs are placed in contact with bone tissue, not only cell adhesion but also support of osteoblast growth has been reported [29–32]. Due to their conductive properties, CNTs help stimulate osteoblastic cells during bone regeneration [33].

The global demand for biomaterials is growing every year. According to Stradvierd Research (the Market Research Report), the total size of the biomaterials market will reach $123 billion in 2021. By 2028, the market is expected to be worth $219 billion. According to the Market Research Report, the orthopedic biomaterials market will be worth USD 19.2 billion in 2022. The compound annual growth rate (CAGR) is expected to remain at 7.8% until 2030.

One of the reasons for the growing demand is the increasing proportion of the aging population. According to the World Health Organization, by 2022, there were more elderly people over the age of sixty than children under the age of five. There has also been an increase in the number of sports injuries. According to National Safety Statistics, there was a 20% increase in injuries in 2021 compared to the previous year.

Among the orthopedic material categories, ceramics was the most popular segment, along with bioglass. This segment accounted for 32.7% of revenue in 2022. The second-fastest growing and currently second-most popular group is polymers, which accounted for the most revenue in 2021. It is expected to dominate the biomaterials market in the coming years.

In addition to the traditional use of biomaterials in orthopedics, the concept of using biomaterials for the early detection of disease is being developed to prevent further progression of the disease. Furthermore, biomaterials used for diagnostics and theragnostics can incorporate scaffolds or nanoparticles, which expand the range of applications [34].

The aim of the presented paper was to determine the composition and conditions for the synthesis of hybrid ceramic–polymer coatings with the characteristics of biomaterials.

The polymeric phase was enriched with MWCNTs to determine the potential of their use as a modifier. Physicochemical analysis, as well as incubation studies, were carried out. These coatings are novel, and so far, no material described in the literature with the same composition and preparation method has been found.

2. Materials and Methods

2.1. Materials

Polyethylene glycol (PEG, Mn = 8000) (Acros Organic, Geel, Belgium) was used for the synthesis of the coatings, poly(ethylene glycol) diacrylate (PEGDA, Mn = 700) was used as a crosslinking agent, and 2-hydroxy-2-methylopropiophenone (Darocur 1173) was used as a photoinitiator (Sigma Aldrich, Darmstadt, Germany). MWCN > 98%, O.D. × L 6–13 nm × 2.5–20 μm (Sigma Aldrich, Darmstadt, Germany) were suspended in a polymer matrix. The components used to create HA were: calcium hydroxide ($Ca(OH)_2$), phosphoric acid V(H_3PO_4 85%), and ammonia water (NH_4OH 25%) (POCH S.A., Gliwice, Poland).

2.2. Methods

2.2.1. Preparation of Hydroxyapatite

The hydroxyapatite used to form composite coatings was obtained using the wet precipitation method. A detailed description of the formation of HA, together with a detailed physiochemical analysis of the powder, was given previously [35].

2.2.2. Preparation of Coatings

A PEG (20%) solution was prepared by mixing the polymer powder with distilled water. Then PEGDA was added to the resulting solution as a crosslinking agent, as well as HA in powder form. The exact addition rates of the substrates used are demonstrated in Table 1. The received solution was homogenized using a Polytron PT 2500 E homogenizer. A photoinitiator was added during the homogenization process using an automatic pipette. Then, 200 μL of the solution obtained was applied and distributed using an automatic pipette to rectangular titanium plates with dimensions of 2 cm × 3 cm. The coatings were exposed to the photocrosslinking process using a Medilux UV 436 HF (Medilux, Korntal-Münchingen, Germany) lamp for 3 min. After the crosslinking process, the coatings were prepared for further testing.

Table 1. Composition of the coatings.

Sample Symbol	PEG 20% [mL]	PEGDA [mL]	HA [g]	Photoinitiator [μL]	MWCNTs [g]
10			-		-
20					-
41	10	1.8		200	0.01
42			0.5		0.02
43					0.03

In total, the compositions of one polymer and four composite coatings with increasing MWCNTs were developed. Carbon nanotubes were added to the polymer solution in solid form and mixed thoroughly to distribute them evenly in the polymer using a homogenization technique. Homogenization ensured good mixing of all components as well as the uniformity of the samples. The MWCNTs were added before adding the hydroxyapatite. The limit value of MWCNTs was 0.03 g, because above this amount, it was not possible to obtain fully crosslinked materials.

Figure 1 presents a scheme for obtaining a composite coating on a Ti-6Al-4V alloy and a photo of an example of the resulting coating.
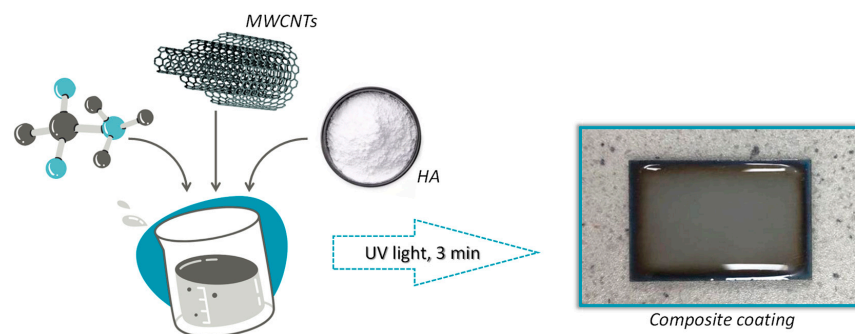
Figure 1. Scheme for obtaining a coating biomaterial.

2.2.3. In Vitro Incubation

The obtained coatings were incubated in vitro at the temperature of 36.6 °C in a POL-EKO incubator, model ST 5 B SMART (Wodzisław Śląski, Poland) for 9 days in artificial saliva, SBF solution, or distilled water. The artificial saliva and SBF compositions are presented in Table 2.

Table 2. Compositions of artificial biological fluids [36].

Artificial Saliva	
Component	**Amount [g/L]**
NaCl	0.400
KCl	0.400
$CaCl_2 \cdot H_2O$	0.795
$Na_2S \cdot 9H_2O$	0.005
$Na_2HPO_4 \cdot H_2O$	0.780
CH_4N_2O	1.000
SBF	
Component	**Amount [g/L]**
NaCl	8.035
$NaHCO_3$	0.355
KCl	0.225
$K_2HPO_4 \cdot 3H_2O$	0.231
$MgCl_2 \cdot 6H_2O$	0.311
1 M HCl	39 mL
$CaCl_2$	0.292
Na_2SO_4	0.072
Tris	8.118

Potentiometric analysis to control the pH value of individual fluids was carried out to evaluate the bioactivity of the resulting composite coatings. Conductometric analysis, measuring the ionic conductivity of the fluids, was carried out simultaneously.

The purpose of these studies was to confirm the interactions occurring between the sample and the incubation medium. An increase in conductivity values suggests ion exchange between the biomaterial and the fluid. This can cause changes in the pH. However, pH changes can also be caused by leaching of individual components from the coatings.

Coatings applied to Ti6Al4V plates were placed in sterile containers filled with fluids. The pH and conductivity values were measured using an Elmetron CX-701 multifunctional device (Zabrze, Poland). Five replicates were performed for each composition.

2.2.4. Morphology Analysis

Morphological studies were carried out on the resulting coatings before and after the incubation period in SBF. A Hitachi TM3000 (Tokyo, Japan) tabletop scanning electron microscope (SEM) equipped with a Quantax 400 V EDS system was used to perform

the morphological analysis. In order to visualize the morphology of the coatings and to capture the potential deposits formed on top of the samples, an EDS microanalysis was also performed. Before SEM measurement, a layer of gold was sputtered onto the surface of the dried sample. However, during the EDS measurement, the presence of Au was not considered in the analyses. Spot EDS analysis was performed to determine the percentage of each element as well as to perform surface mapping.

2.2.5. FT-IR Analysis

Fourier-transform infrared spectroscopy (FT-IR) was used to determine the functional groups and analyze the composition before and after incubation. A Thermo Scientific Nicolet iS5 FTIR (Loughborough, UK) spectrophotometer equipped with an iD7 was used. Due to the monolithic diamond crystal, there is a high optical contact between the sample and the diamond, leading to a clear spectrum. The wavelength range recorded was 4000–400 cm^{-1}. The study was performed at room temperature with conditions of 32 scans at 4.0 cm^{-1} resolution. The FT-IR spectra were collected for three random locations on the surface of each sample.

3. Results

3.1. In Vitro Incubation

3.1.1. pH Metric Analysis

During in vitro incubation, pH changes were measured in the solutions to determine the stability of the coatings under conditions similar to the human body. The exact results of the test are demonstrated in Figure 2. It was observed that coatings with HA had a more alkaline character than unsupplemented ones. This is related to the washing-out process of hydroxyapatite, which results in a hardly soluble precipitate [35].
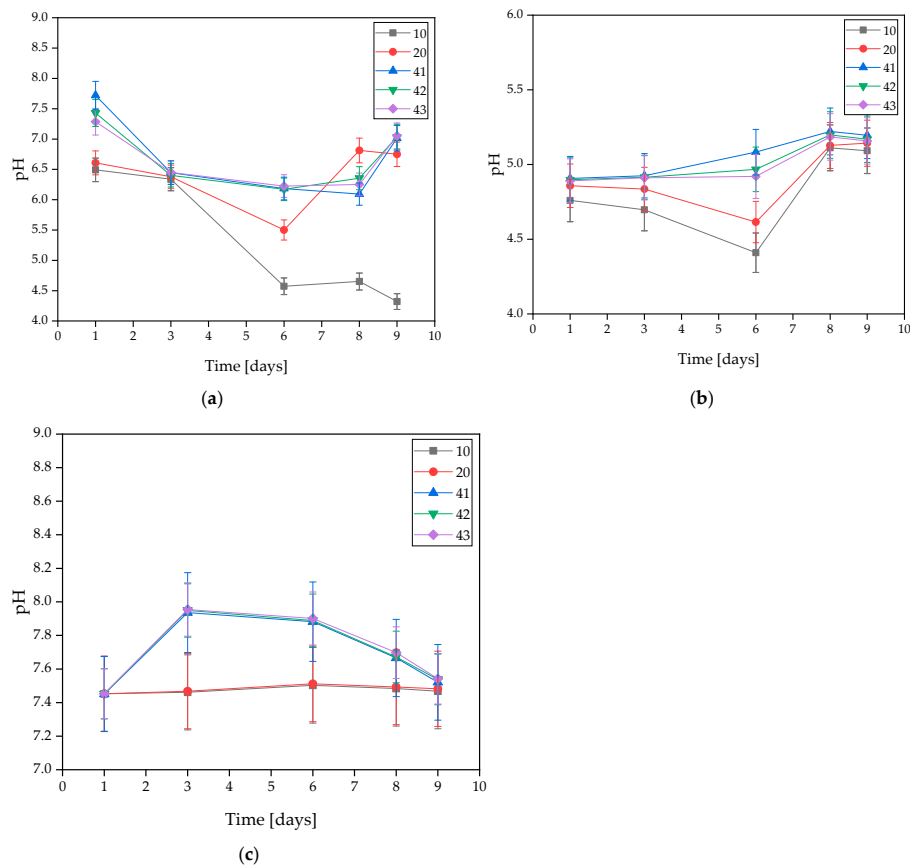

Figure 2. Measured pH values of coatings incubated in (**a**) distilled water, (**b**) artificial saliva, or (**c**) SBF solution.

On the basis of the MWCNTs-containing samples tested, it was found that the presence of nanotubes in the coating caused changes in the pH value of the solutions. The only rapid change in pH level observed was in the SBF solution during the 3 days of incubation, and its value was the highest at that point. For all three samples, the pH level remained between 7.939 and 7.955. However, a stabilization of the process was observed at later stages.

In the artificial saliva solution, the pH value increased gradually throughout the incubation. Samples immersed in distilled water exhibited a slight change in pH throughout the entire incubation. This is due to the high purity of the water, which results in a low concentration of free ions reacting with the coating and causing significant pH changes. Spikes in pH values in water are likely due to leaching of residual uncrosslinked polymer from the interior of the material. Smaller pH shifts in SBF may be due to its buffering nature. On this basis, it was concluded that the addition of MWCNTs caused a slight increase in pH value.

The stability of the resulting coatings in all solutions was also observed due to a lack of large pH changes throughout the entire incubation process. An interesting behavior of the materials was observed for SBF, as the pH value curves for coatings without MWCNTs, i.e., 10 and 20, almost completely overlap, while the pH values for coatings containing MWCNTs, i.e., 41, 42, and 43, also overlap, but reach slightly higher values. This suggests that despite the buffering properties that SBF possesses, even a small presence of carbon nanotubes affects the pH change. However, the values are still within safe limits for the body.

3.1.2. Conductivity Analysis

The incubated samples were subjected to an electrolyte conductivity test. The exact results are presented in Figure 3. This test is based on the changes in the ion concentration in the solution.
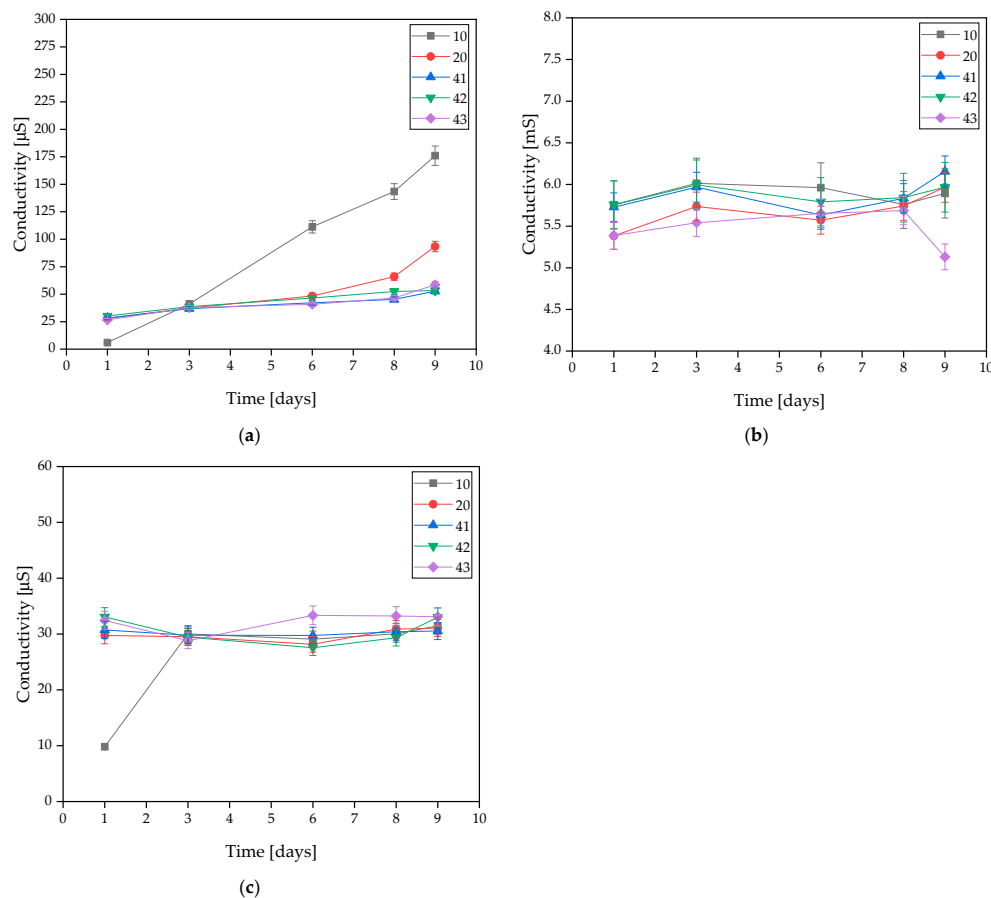

Figure 3. Measured conductivity values of coatings incubated in (**a**) distilled water, (**b**) artificial saliva, or (**c**) SBF solution.

Measurements for samples 10 and 20 demonstrated that the addition of HA resulted in a minimal improvement in stability and, in the case of distilled water, a slight decrease in conductivity. For coatings containing MWCNTs, in distilled water, the samples revealed very strong stability throughout the incubation process. This is due to the low concentration of free ions in the distilled water. Minimal conductivity changes were observed in the SBF solution, but these were low enough to conclude that the materials were stable in this solution. The same conclusion was reached with the artificial saliva solution. The conductivity of the sample increased minimally without sudden changes. This is related to the degradation process, which is more intense than in the other solutions.

3.2. Morphology Analysis
3.2.1. Coatings Morphology before Incubation

Figure 3 presents images of the surface morphology before incubation in artificial saliva and SBF solution. Figure 4b demonstrates a change in the surface morphology due to HA crystals suspended in the polymer area, while surface Figure 4a is completely smooth. On the surfaces Figure 4c–e, these crystals are also visible. The surface areas for Figure 4a,b were also compared to an earlier publication with l-cysteine modified coatings [35].
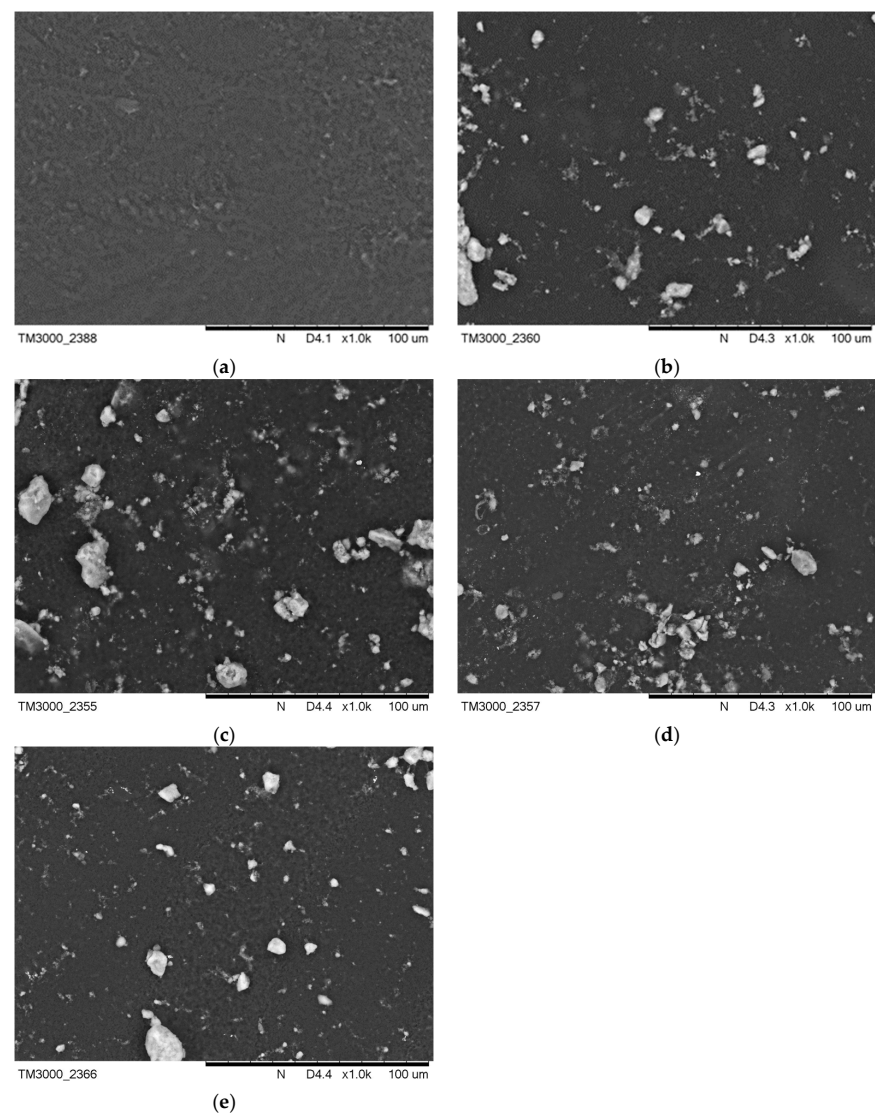

Figure 4. SEM images of (**a**) PEG-based coating 10, (**b**) PEG coating containing HA, (**c**) coating with 0.01 g CNTs, (**d**) coating with 0.02 g CNTs, and (**e**) coating with 0.03 g CNTs.

3.2.2. Coatings Morphology after Incubation

After the incubation process, changes were observed in the coatings of the samples containing MWCNTs. Images after incubation of the samples are demonstrated in Figures 5 and 6.
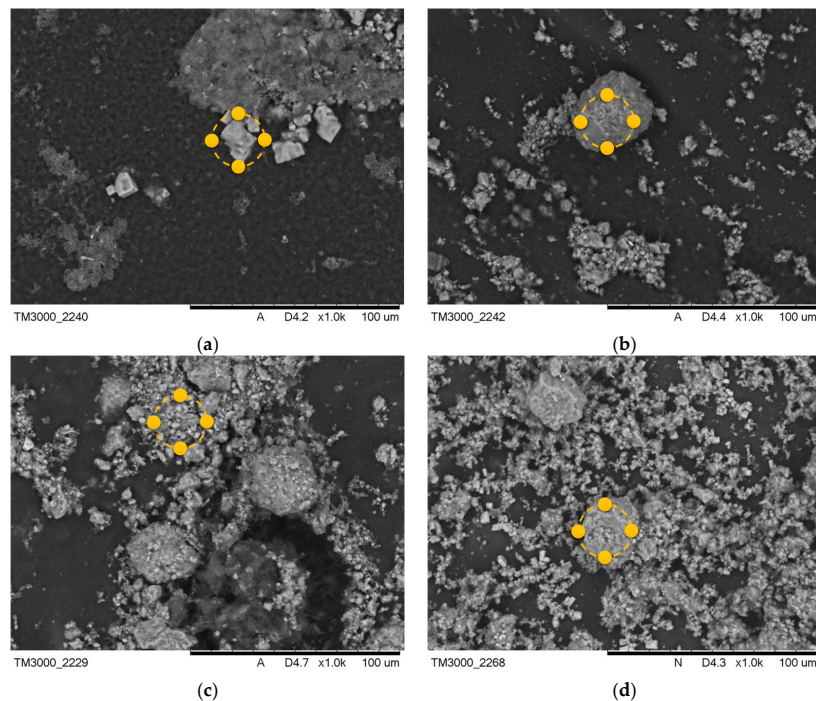

Figure 5. SEM images of samples after incubation in SBF solution (**a**) PEG-based coating 10, (**b**) PEG coating containing HA, (**c**) coating with 0.02 g CNTs, and (**d**) coating with 0.03 g CNTs. Yellow markers indicate the location of the EDS elemental analysis.
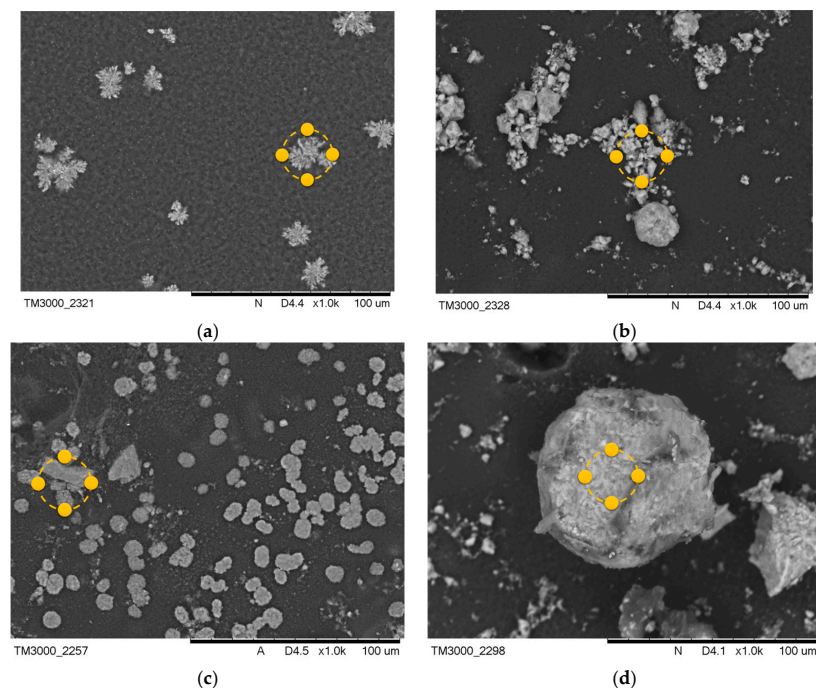

Figure 6. SEM images of samples after incubation in artificial saliva (**a**) PEG-based coating 10, (**b**) PEG coating containing HA, (**c**) coating with 0.02 g CNTs, (**d**) coating with 0.03 g CNTs. Yellow markers indicate the location of the EDS elemental analysis.

The formation of pits and grooves was observed on the surfaces, indicating the recrystallization process of the apatite. In all samples containing CNTs incubated in SBF solution, the appearance of large agglomerations of apatite crystals was noted. This is related to the specificity of the SBF solution, which simulates a human plasma environment with a high ion concentration. Calcium ions react with negative HA, later involving a phosphorus ion. This results in the compound being converted into apatite [33]. In biomaterials incubated in artificial saliva, the formation of a visible accumulation of apatite crystals was observed, as in the SBF solution.

Along with the morphological examination, an EDS microanalysis was performed. Its purpose was to identify the elements present and to determine their abundance in the coating. The exact results of the microanalysis are presented in Tables 3 and 4. The most frequent elements present were C and O. This indicates the chemical composition of the polymer that was used. Na and Cl ions were also observed. This appears to indicate that the biomaterial reacts with the solution in which it is incubated. The presence of Ca and P in the biomaterial results in the coatings having a bioactive property. The presence of Ca and P in material 10 after the incubation period is due to the composition of the incubation fluids, as the fluids contained trace amounts of these elements.

Table 3. Elemental composition of the tested coatings after incubation in SBF solution.

Sample	Mass Percentage [w%]
10	C: 45.88, O: 19.31, Cl: 19.06, Na: 14.00, Ca: 1.33, P: 0.42
20	O: 45.33, Ca: 24.87, C: 16.55, P: 9.45, Cl: 2.53, Na: 0.8
42	O: 41.14, Ca: 29.88, C: 13.87, P: 9.89, Cl: 4.39, Na: 0.74
43	C: 21.79, O: 42.48, Ca: 18.77, P: 8.58, Cl: 4.44, Na: 3.93

Table 4. Elemental composition of the tested coatings after incubation in artificial saliva.

Sample	Mass Percentage [w%]
10	C: 40.29, O: 39.57, Ca: 11.03, P: 7.03, Cl: 1.68, Na: 0.39
20	O: 46.15, C: 28.64, Ca: 15.91, P: 7.12, Cl: 1.52, Na: 0.65
42	C: 43.69, O: 35.86, Ca: 13.14, P: 3.95, Cl: 2.31, K: 1.04, Na: 0.01
43	O: 47.94, C: 23.94, Ca: 17.56, P: 8.77, Cl: 0.96, Na: 0.82

Considering that in the context of orthopedic applications, behavior in the SBF fluid is a more important indicator that provides information regarding the application potential, EDS microanalysis with mapping of individual elements was performed, as can be observed in Figure 6. Elements such as Ca and P were marked on the mapping, confirming the presence of calcium phosphate, such as HA, in the material, as well as the formation of new apatite layers on the surface due to interactions with SBF fluid. Figure 7a,b clearly illustrate the overlap on the surface.

The presence of Na, Mg, or Cl is a direct result of the composition of the SBF fluid, as these ions are present in the salts used to prepare it. The overlap of the spectrum of Mg with Cl or Na with Cl may indicate the formation of chlorides. This is also evidenced by the characteristic geometric shape of the crystals formed.
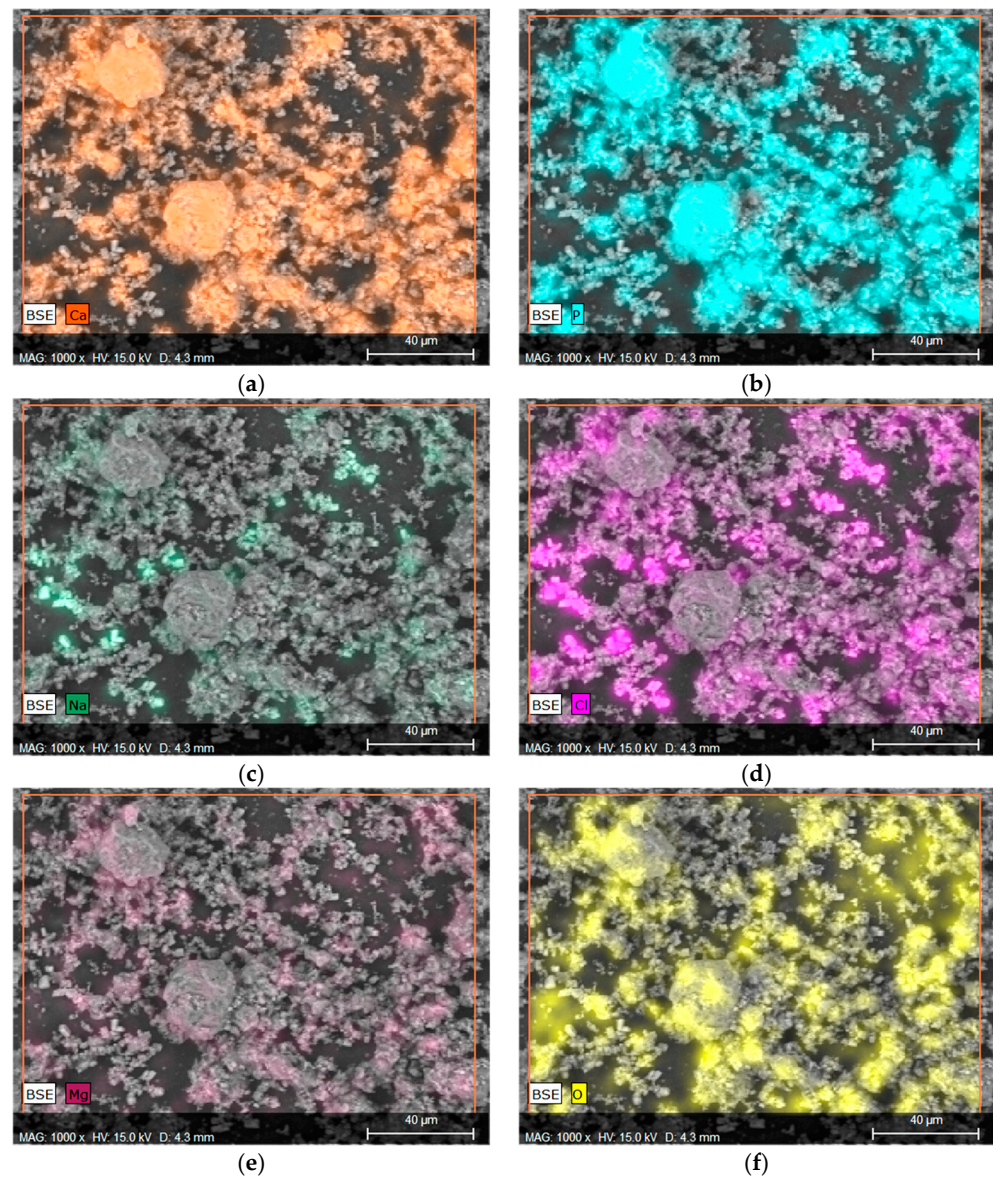
Figure 7. Elemental EDS microanalysis and determination of elements on the surface of material 43 after incubation in SBF (**a**) calcium, (**b**) phosphorus, (**c**) sodium, (**d**) chlorine, (**e**) magnesium, and (**f**) oxygen.

3.3. FT-IR Analysis

3.3.1. Spectrum of Coatings before Incubation

Using FT-IR spectrometric analysis to determine the chemical composition of the resulting coatings, the biomaterial spectra are demonstrated in Figure 8. The spectra of the coatings presented are PEG, PEG with hydroxyapatite, and also coatings containing 0.01 g, 0.02 g, or 0.03 g of nanotubes. The spectra of pure hydroxyapatite and pure PEG are presented in publications related to the studies performed and are described in this article [36]. For all samples that are shown, a peak was observed at a wavelength of 1100 cm^{-1} and 3500 cm^{-1}, originating from the OH group associated with the presence of the polymer. In samples containing HA, a characteristic peak related to PO$_4^{3-}$ oscillation was observed at a wavelength of 560 cm^{-1}. In coatings containing CNTs, the featured peaks were more pronounced. This behavior was observed at wavenumbers of 1030 cm^{-1} and 560 cm^{-1}, respectively.
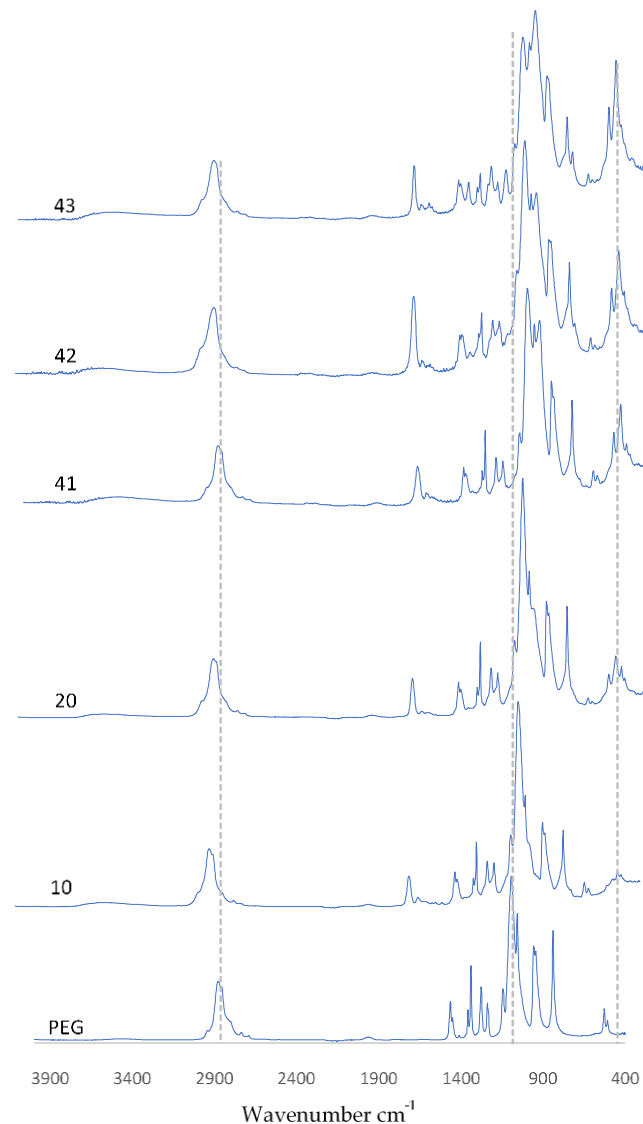
Figure 8. FT-IR spectra of coatings before incubation.

Finally, it is significant that FT-IR spectra were collected for three random locations on the surface of each sample. The spectra overlapped, which suggests that all of the coatings were homogeneous. Otherwise, the individual peaks would not have overlapped, or shifts would have been observed.

3.3.2. Spectrum of Coatings after Incubation

After a 9-day incubation carried out in SBF solution, artificial saliva, or distilled water, FT-IR analysis was carried out. Figure 9 shows the obtained spectra of the incubated coatings. An increase in absorbance was observed for the peak at wavelength 1730 cm^{-1}. For samples 10 and 20 incubated in SBF solution, the vibration modulus increased in the range of 700 cm^{-1}–400 cm^{-1}. In the spectra of coatings containing nanotubes, there was a decrease in the number of visible peaks. It should be noted that the diagrams overlap with the spectra obtained for the coatings before incubation. This suggests that as a result of incubation, at the coating–incubation fluid interface, there are no potential degradation or destruction processes of the composition.
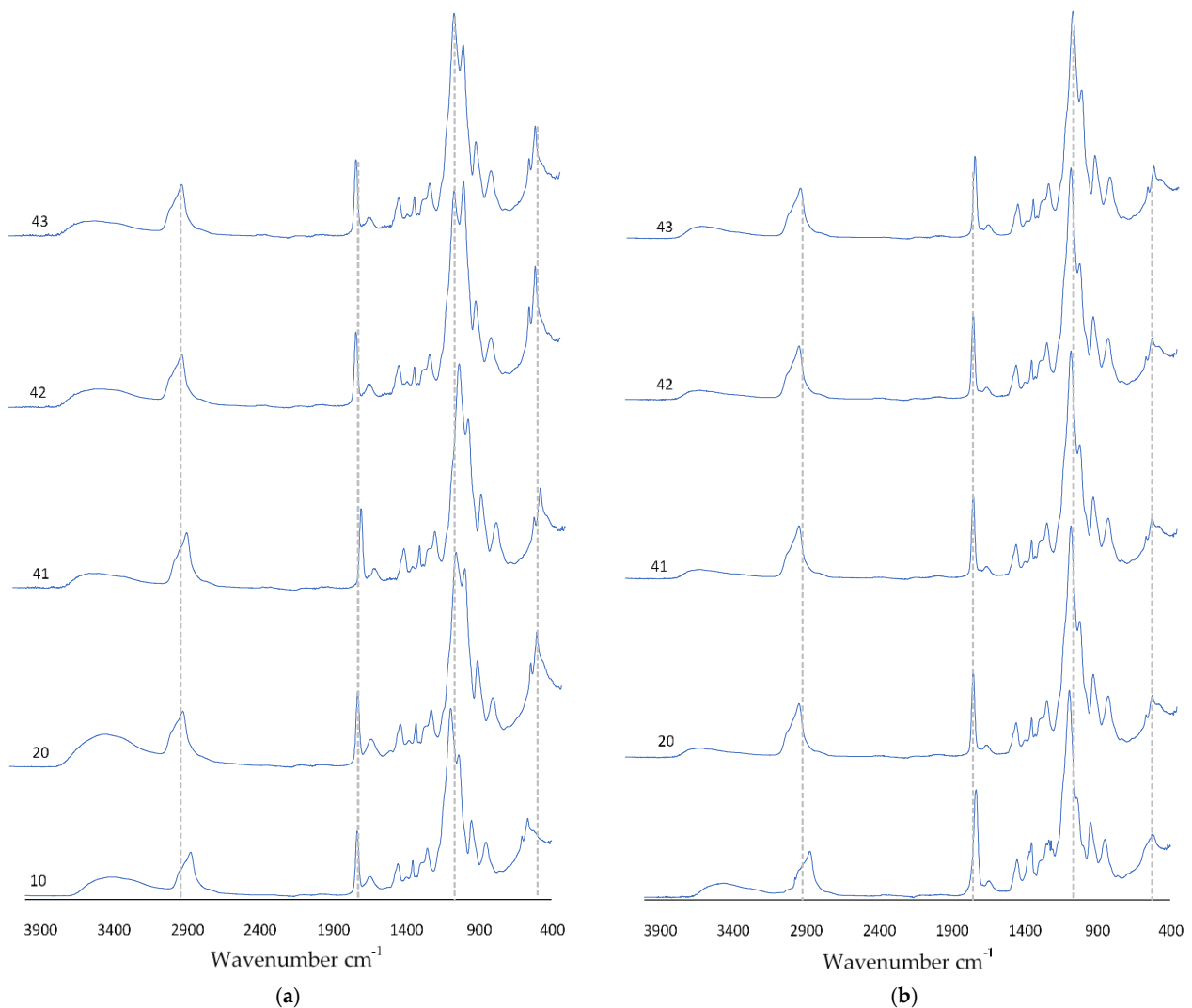
Figure 9. FT-IR spectra of coatings after incubation in (**a**) SBF solution or (**b**) artificial saliva.

4. Discussion

The results of this study confirm that the ceramic–polymer coating containing nanotubes can potentially be used as a biomaterial to support bone tissue regeneration. A 9-day in vitro study was performed to determine the effect of the coatings on the environment of artificial body fluids in terms of changing pH values and conductivity. The results of this study indicate proper interactions of the coatings with the solutions in which they were incubated.

In samples containing hydroxyapatite, the pH value increased minimally in the alkaline direction, which is related to the characteristics of the HA. A conductivity test verified the interaction of the coating ions with the ions of the prepared solutions, indicating a proper interaction without rapid changes throughout the incubation period. The changes in the pH and conductivity values confirm that the developed coatings are not inert and interact with the selected fluids. However, these interactions do not cause degradation or destruction of the coating surfaces, as confirmed by the overlapping FTIR spectra.

Morphological studies, together with EDS microanalysis, were carried out to determine the changes in the coatings caused by the incubation, and to identify and quantify the elements present. On the basis of this study, apatite agglomerations were found to appear on the surface of the samples, formed due to ion reactions between the HA and the solution. The microanalysis confirmed the occurrence of calcium and phosphorus. Elemental mappings in particular confirmed the formation of new calcium phosphate values. This effect was likely further supported by the presence of these ions in the composition of the

SBF fluid. The other elements appearing are related to the structure of the polymer and the normal reactions of the coatings with the solutions.

FT-IR spectrometric examination confirmed the occurrence of the functional groups associated with the substrates used through the appearance of characteristic peaks, revealing the chemical composition of the biomaterial.

The performed studies were compared with similar research in terms of the connection between carbon nanotubes and hydroxyapatite. The selected studies had differences in the method of coating synthesis. Despite the mentioned difference, similarities in the form of proper bonding of HA to the surface of the nanotubes was demonstrated [37–39].

5. Conclusions

In the presented study, the synthesis of coatings that have the potential to support bone tissue regeneration is reported. The technique developed was based on the use of UV light and enabled us to obtain composite coatings on titanium plates under UV light. The selected parameters, i.e., crosslinking time and the types of crosslinking agents and photoinitiators, made it possible to obtain completed materials with satisfactory organoleptic properties (without roughness or holes, fully continuous and crosslinked). This study confirmed that the addition of nanotubes to a ceramic–polymer base had no negative effect on the results during incubation in biological fluids. Coatings containing MWCNTs demonstrated bioactivity, which is an important feature of a biomaterial. Bioactivity was confirmed by observing new apatite layers that appeared following incubation. Further biological studies should focus on the reactions of cells in contact with the coatings in order to determine whether the biomaterial influences the adhesion and growth of bone tissue.

Author Contributions: Conceptualization, D.T. and D.S.; methodology, D.S. and W.F.; software, D.T. and K.N.; validation, D.S., W.F. and K.N.; formal analysis, D.S. and W.F.; investigation, D.S. and W.F.; resources, W.F.; data curation, D.S.; writing—original draft preparation, D.T.; writing—review and editing, A.S.-K., D.S. and K.N.; visualization, D.T. and D.S.; supervision, A.S.-K.; project administration, A.S.-K.; funding acquisition, A.S.-K. All authors have read and agreed to the published version of the manuscript.

Institutional Review Board Statement: Not applicable.

Informed Consent Statement: Not applicable.

Data Availability Statement: Data that support the findings of this study are contained within the article.

Conflicts of Interest: The authors declare no conflict of interest.

Abbreviations

Abbreviations	Description
HA	Hydroxyapatite
PEG	Polyethylene Glycols
CNTs	Carbon Nanotubes
SWCNTs	Single-Walled Carbon Nanotubes
MWCNTs	Multi-Walled Carbon Nanotubes
PEGDA	Poly(ethylene glycol) Diacrylate
SBF	Simulated Body Fluid
XRD	X-ray Diffraction Analysis
EDS	Energy Dispersive X-ray Spectroscopy
FT-IR	Fourier Transform Infrared Spectroscopy

References

1. Hill, P.A. Bone Remodelling. *Br. J. Orthod.* **1998**, *25*, 101–107. [CrossRef] [PubMed]
2. Rachner, T.D.; Khosla, S.; Hofb, L.C. Osteoporosis: Now and the Future. *Lancet* **2011**, *377*, 1276–1287. [CrossRef]
3. Johnson, R.J. Overuse Injuries in Sports: A Review. *Sports Med.* **1985**, *2*, 316–333.
4. Gibson, I.R.; Ke, S.; Best, S.M.; Bonfield, W. Effect of Powder Characteristics on the Sinterability of Hydroxyapatite Powders. *J. Mater. Sci. Mater. Med.* **2001**, *12*, 163–171. [CrossRef] [PubMed]
5. Moroni, A.; Caja, V.L.; Egger, E.L.; Trinchese, L.; Chao, E.Y.S. Histomorphometry of Hydroxyapatite Coated and Uncoated Porous Titanium Bone Implants. *Biomaterials* **1994**, *15*, 926–930. [CrossRef] [PubMed]
6. Tracy, B.M.; Doremus, R.H. Direct Electron Microscopy Studies of the Bone-Hydroxylapatite Interface. *J. Biomed. Mater. Res.* **1984**, *18*, 719–726. [CrossRef] [PubMed]
7. Kato, K.; Sc, D.; Aoki, H.; Eng Tabata, D.T.; Do, D.S.; Ogiso, M. Biocompatibility of Apatite Ceramics in mandibles. *Biomater. Med. Devices Artif. Organs* **1979**, *7*, 291–297. [CrossRef]
8. Silva, P.L.; Santos, J.D.; Monteiro, F.J.; Knowles, J.C. Adhesion and Microstructural Characterization of Plasma-Sprayed Hydroxyapatite/Glass Ceramic Coatings onto Ti-6A1-4V Substrates. *Surf. Coat. Technol.* **1998**, *102*, 191–196. [CrossRef]
9. Qiu, C.; Xiao, X.; Liu, R. Biomimetic Synthesis of Spherical Nano-Hydroxyapatite in the Presence of Polyethylene Glycol. *Ceram. Int.* **2008**, *34*, 1747–1751. [CrossRef]
10. Venkatasubbu, G.D.; Ramasamy, S.; Avadhani, G.S.; Ramakrishnan, V.; Kumar, J. Surface Modification and Paclitaxel Drug Delivery of Folic Acid Modified Polyethylene Glycol Functionalized Hydroxyapatite Nanoparticles. *Powder Technol.* **2013**, *235*, 437–442. [CrossRef]
11. Photos, P.J.; Bacakova, L.; Discher, B.; Bates, F.S.; Discher, D.E. Polymer Vesicles in Vivo: Correlations with PEG Molecular Weight. *J. Control Release* **2003**, *90*, 323–334. [CrossRef]
12. Mironov, S.; Sato, Y.S.; Kokawa, H. Friction-Stir Welding and Processing of Ti-6Al-4V Titanium Alloy: A Review. *J. Mater. Sci. Technol.* **2018**, *34*, 58–72. [CrossRef]
13. Okazaki, Y.; Nishimura, E.; Nakada, H.; Kobayashi, K. Surface analysis of Ti–15Zr–4Nb–4Ta Alloy after Implantation in Rat Tibia. *Biomaterials* **2001**, *22*, 599–607. [CrossRef]
14. Heinl, P.; Müller, L.; Körner, C.; Singer, R.F.; Müller, F.A. Cellular Ti-6Al-4V Structures with Interconnected Macro Porosity for Bone Implants Fabricated by Selective Electron Beam Melting. *Acta. Biomater.* **2008**, *4*, 1536–1544. [CrossRef] [PubMed]
15. Okazaki, Y.; Rao, S.; Ito, Y.; Tateishi, T. Corrosion Resistance, Mechanical Properties, Corrosion Fatigue Strength and Cytocompatibility of New Ti Alloys without Al and V. *Biomaterials* **1998**, *19*, 1197–1215. [CrossRef] [PubMed]
16. Mohseni, E.; Zalnezhad, E.; Bushroa, A.R.; Hamouda, A.M.; Goh, B.T.; Yoon, G.H. Ti/TiN/HA Coating on Ti–6Al–4V for Biomedical Applications. *Ceram. Int.* **2015**, *41*, 14447–14457. [CrossRef]
17. Ponader, S.; Von Wilmowsky, C.; Widenmayer, M.; Lutz, R.; Heinl, P.; Körner, C.; Singer, R.F.; Nkenke, E.; Neukam, F.W.; Schlegel, K.A. In Vivo Performance of Selective Electron Beam-Melted Ti-6Al-4V Structures. *J. Biomed. Mater. Res. A* **2010**, *92*, 56–62. [CrossRef]
18. Long, M.; Rack, H.J. Titanium Alloys in Total Joint Replacement—A Materials Science Perspective. *Biomaterials* **1998**, *19*, 1621–1639. [CrossRef]
19. Li, J.P.; Li, S.H.; Van Blitterswijk, C.A.; De Groot, K. A Novel Porous Ti6A14V: Characterization and Cell Attachment. *J. Biomed. Mater. Res. A* **2005**, *73*, 223–233. [CrossRef]
20. Wilke, A.; Landgraff, M.; Orth, J.; Poenitz, H.; Kienapfel, H.; Boelte, K.; Franke, R.P. Human Bone Marrow Cell Culture: A Sensitive Method for Determination of the Biocompatibility of Implant Materials. *Altern. Lab. Anim.* **1999**, *27*, 137–151. [CrossRef]
21. Pei, B.; Wang, W.; Dunne, N.; Li, X. Applications of Carbon Nanotubes in Bone Tissue Regeneration and Engineering: Superiority, Concerns, Current Advancements, and Prospects. *Nanomaterials* **2019**, *9*, 1501. [CrossRef]
22. Mattioli-Belmonte, M.; Vozzi, G.; Whulanza, Y.; Seggiani, M.; Fantauzzi, V.; Orsini, G.; Ahluwalia, A. Tuning Polycaprolactone-Carbon Nanotube Composites for Bone Tissue Engineering Scaffolds. *Mater. Sci. Eng. C* **2012**, *32*, 152–159. [CrossRef]
23. Venkatesan, J.; Pallela, R.; Kim, S.K. Applications of Carbon Nanomaterials in Bone Tissue Engineering. *J. Biomed. Nanotechnol.* **2014**, *10*, 3105–3123. [CrossRef] [PubMed]
24. Mohan, V.B.; Lau, K.T.; Hui, D.; Bhattacharyya, D. Graphene-Based Materials and Their Composites: A Review on Production, Applications and Product Limitations. *Compos. B Eng.* **2018**, *142*, 200–220. [CrossRef]
25. Pantano, A.; Parks, D.M.; Boyce, M.C. Mechanics of Deformation of Single- and Multi-Wall Carbon Nanotubes. *J. Mech. Phys. Solids* **2004**, *52*, 789–821. [CrossRef]
26. Hu, H.; Ni, Y.; Montana, V.; Haddon, R.C.; Parpura, V. Chemically Functionalized Carbon Nanotubes as Substrates for Neuronal Growth. *Nano Lett.* **2004**, *4*, 507–511. [CrossRef] [PubMed]
27. Chłopek, J.; Czajkowska, B.; Szaraniec, B.; Frackowiak, E.; Szostak, K.; Béguin, F. In Vitro Studies of Carbon Nanotubes Biocompatibility. *Carbon N. Y.* **2006**, *44*, 1106–1111. [CrossRef]
28. Wang, W.; Yokoyama, A.; Liao, S.; Omori, M.; Zhu, Y.; Uo, M.; Akasaka, T.; Watari, F. Preparation and Characteristics of a Binderless Carbon Nanotube Monolith and Its Biocompatibility. *Mater. Sci. Eng. C* **2008**, *28*, 1082–1086. [CrossRef]
29. Akasaka, T.; Yokoyama, A.; Matsuoka, M.; Hashimoto, T.; Abe, S.; Uo, M.; Watari, F. Adhesion of Human Osteoblast-like Cells (Saos-2) to Carbon Nanotube Sheets. *Biomed. Mater. Eng.* **2009**, *19*, 147–153. [CrossRef]

30. Aoki, N.; Yokoyama, A.; Nodasaka, Y.; Akasaka, T.; Uo, M.; Sato, Y.; Tohji, K.; Watari, F. Cell Culture on a Carbon Nanotube Scaffold. *J. Biomed. Nanotechnol.* **2006**, *1*, 402–405. [CrossRef]
31. Terada, M.; Abe, S.; Akasaka, T.; Uo, M.; Kitagawa, Y.; Watari, F. Development of a Multiwalled Carbon Nanotube Coated Collagen Dish. *Dent. Mater. J.* **2009**, *28*, 82–88. [CrossRef] [PubMed]
32. Kroustalli, A.A.; Kourkouli, S.N.; Deligianni, D.D. Cellular Function and Adhesion Mechanisms of Human Bone Marrow Mesenchymal Stem Cells on Multi-Walled Carbon Nanotubes. *Ann. Biomed. Eng.* **2013**, *41*, 2655–2665. [CrossRef] [PubMed]
33. Saito, N.; Usui, Y.; Aoki, K.; Narita, N.; Shimizu, M.; Hara, K.; Ogiwara, N.; Nakamura, K.; Ishigaki, N.; Kato, H.; et al. Carbon Nanotubes: Biomaterial Applications. *Chem. Soc. Rev.* **2009**, *38*, 1897–1903. [CrossRef] [PubMed]
34. Ackun-Farmmer, M.A.; Overby, C.T.; Haws, B.E.; Choe, R.; Benoit, D.S.W. Biomaterials for Orthopedic Diagnostics and Theranostics. *Curr. Opin. Biomed. Eng.* **2021**, *19*, 100308. [CrossRef] [PubMed]
35. Słota, D.; Florkiewicz, W.; Sobczak-Kupiec, A. Ceramic-Polymer Coatings on Ti-6Al-4V Alloy Modified with L-Cysteine in Biomedical Applications. *Mater. Today Commun.* **2020**, *25*, 101301. [CrossRef]
36. Slota, D.; Głąb, M.; Tyliszczak, B.; Dogulas, T.E.L.; Rudnicka, K.; Miernik, K.; Urbaniak, M.M.; Rusek-Wala, P.; Sobczak-upiec, A. Composites Based on Hydroxyapatite and Whey Protein Isolate for Applications in Bone Regeneration. *Materials* **2021**, *14*, 2317. [CrossRef]
37. Malekahmadi, O.; Kalantar, M.; Nouri-Khezrabad, M. Effect of Carbon Nanotubes on the Thermal Conductivity Enhancement of Synthesized Hydroxyapatite Filled with Water for Dental Applications: Experimental Characterization and Numerical Study. *J. Therm. Anal. Calorim.* **2021**, *144*, 2109–2126. [CrossRef]
38. Park, J.E.; Jang, Y.S.; Bae, T.S.; Lee, M.H. Biocompatibility Characteristics of Titanium Coated with Multiwalled Carbon Nanotubes-Hydroxyapatite Nanocomposites. *Materials* **2019**, *12*, 224. [CrossRef]
39. Balani, K.; Anderson, R.; Laha, T.; Andara, M.; Tercero, J.; Crumpler, E.; Agarwal, A. Plasma-Sprayed Carbon Nanotube Reinforced Hydroxyapatite Coatings and Their Interaction with Human Osteoblasts in Vitro. *Biomaterials* **2007**, *28*, 618–624. [CrossRef]